A&A 412, 727–734 (2003)
DOI: 10.1051/0004-6361:20031276

Astronomy & Astrophysics

H_2 excitation imaging of the Orion Molecular Cloud⋆

L. E. Kristensen[1], M. Gustafsson[1], D. Field[1,⋆⋆], G. Callejo[2,3], J. L. Lemaire[2,3,⋆⋆], L. Vannier[2], and G. Pineau des Forêts[4]

[1] Department of Physics and Astronomy, University of Aarhus, 8000 Aarhus C, Denmark
[2] Observatoire de Paris-Meudon, LERMA and UMR 8112 of the CNRS, 92195 Meudon Principal Cedex, France
[3] Université de Cergy-Pontoise, LERMA and UMR 8112 of the CNRS, 95806 Cergy Cedex, France
[4] Institut d'Astrophysique Spatiale, Université Paris XI, 91405 Orsay Cedex, France

Received 30 January 2003 / Accepted 11 August 2003

Abstract. Observations are reported of IR emission in H_2, around 2 μm in the K-band, obtained with the ESO 3.6 m telescope using the ADONIS adaptive optics system. Data cover a region of the Orion Molecular Cloud north of the Trapezium stars and SW of the Becklin-Neugebauer object. Excellent seeing yielded diffraction limited images in the $v = 2{-}1$ S(1) line at 2.247 μm. Excitation temperature images were created by combining these data with similar data for H_2 emission in the $v = 1{-}0$ S(1) line reported earlier (Vannier et al. 2001). Shock models are used to estimate densities in emitting clumps of material. In local zones with high excitation temperatures, post-shock densities are found to be as high as several times 10^8 cm^{-3}, an order of magnitude denser than our previous estimates. We propose that the nature of these zones is dictated by the combined activity of shocks, which create dense structures, and the powerful radiation field of θ^1C Ori which photoevaporates the boundaries of these structures.

Key words. ISM: individual objects: OMC1 – ISM: kinematics and dynamics – ISM: molecules – shock waves – ISM: lines and bands

1. Introduction

The Orion Molecular Cloud, OMC1, lying at the heart of the Orion Nebula (Ferland 2001; O'Dell 2001), is a region in which powerful outflows from massive young stars interact strongly with the parent gas from which they formed. This contributes, it is believed, to the formation of further massive stars (Elmegreen & Lada 1977) and an extensive population of low mass stars. The Trapezium cluster and the region around it, which includes both OMC1 and the Becklin-Neugebauer (BN) object, itself a young and massive B-star (Gezari et al. 1998), contains several hundred very early low mass stars within a region of scale 0.5 pc. The age of the cluster is of the order of 10^6 years (Hillenbrand 1997; Palla & Stahler 1999; Luhman et al. 2000).

An understanding of how massive stars influence the formation of compact bodies in the surrounding gas is based on the hypothesis that outflows from massive stars may shock-compress the local gas, triggering the formation of stars, brown dwarfs or free-floating objects of planetary mass (Lucas & Roche 2000; Zapatero Osorio et al. 2000; Boss 2001). This mechanism, if operational, has far-reaching consequences for star formation in many regions of the Galaxy and in external galaxies, making an important contribution to the initial mass function (IMF) for objects in the low mass range. The Galactic IMF has been extensively studied, especially in Orion, e.g. Luhman et al. (2000), in which studies extend down to 0.02 $M_\odot$.

In recent work (Vannier et al. 2001, hereafter V2001), we attempted quantitatively to test the shock compression hypothesis in OMC1, examining the distribution of scale sizes of regions brightly emitting in H_2 (e.g. Allen & Burton 1993; Schild et al. 1997; Chen et al. 1998; Stolovy et al. 1998; Schultz et al. 1999) and using theoretical shock models (Wilgenbus et al. 2000) to reproduce the observed brightness of emission in the H_2 $v = 1{-}0$ S(1) line at 2.121 μm. The results in V2001 showed that clumps of gas emitting in the $v = 1{-}0$ S(1) line do not form a fractal size distribution but rather display a preferred scale size lying between 1.″4 to 1.″8, that is $3{\times}10^{-3}$ to $4{\times}10^{-3}$ pc given a distance to Orion of 460 pc (Bally et al. 2000). It was found that the passage of magnetic (C-type) shocks, with velocities of ∼30 kms^{-1}, impinging on gas of preshock number density 10^6 cm^{-3}, could yield the very bright H_2 emission observed. The passage of the shock was found to compress gas to number densities ($n_H + 2n_{H_2}$) of several times 10^7 cm^{-3}. V2001 found that one clump in the field (region 1, below) may be

Send offprint requests to: D. Field,
e-mail: dfield@phys.au.dk

⋆ Mainly based on observations performed at the ESO/La Silla 3.6 m telescope. Reference is also made to observations performed at the CFHT 3.6 m telescope.

⋆⋆ Visiting astronomer at the European Southern Observatory, La Silla, Chile.

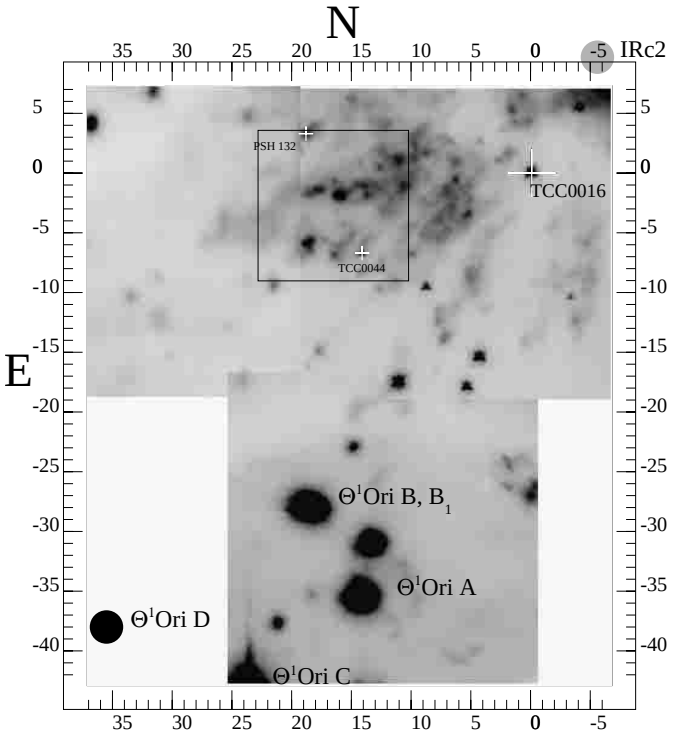

Fig. 1. A finding chart, recorded at 2.121 μm (H_2 emission + continuum), showing the area in which observations are presented, extending approximately from 11″ to 23″ to the East, 3″ to the North and 9″ to the south of TCC0016 (marked as a large white cross). TCC0016 lies at $05^h35^m14^s.91$, –05°22′39.″31 (J2000). The positions of the Trapezium stars and IRc2 are also shown relative to TCC0016. Two stars used for image registration, PSH132 and TCC0044 located at 19″E, 3″N and 14″E, 7″S of TCC0016, are also indicated. The box identifies the zone studied in the present work.

gravitationally unstable and may be a potential site for future low mass star formation. This result is consistent with the stellar density in the Trapezium cluster, which would yield one star on average in the volume of gas observed (Luhman et al. 2000).

In the present work we consider, as in V2001, a small part of OMC1 in a region centered ∼45″ north of the Trapezium cluster, reporting data in the $v = 2{-}1$ S(1) line at 2.247 μm, at high spatial resolution, obtained using adaptive optics.

2. Observations and data reduction

A finding chart for the region observed, recorded in the $v = 1{-}0$ S(1) line, is given in Fig. 1. The brightest H_2 emission is centered around 10″ E of the reference star TCC0016 and is the region originally designated as "Peak 2" in Beckwith et al. (1978). BN lies 20.″3 to the north-west of TCC0016, that is, 0.045 pc.

The ADONIS Adaptive Optics (AO) system at the ESO 3.6 m telescope was used for the observations, which took place on 27th to 29th December 1996. ADONIS was equipped with the infra-red Sharp-NICMOS camera (256 × 256 pixels). At the time of our observations the seeing was exceptionally good, lying between 0.3 and 0.4 arcsec, and the lens set was used which gave a resolution of 50 mas/pixel, with a field of view of 12.8″ × 12.8″. Data recorded here in the H_2 $v = 2{-}1$ S(1) line are used in conjunction with data in $v = 1{-}0$ S(1), where the latter have already been reported in V2001. In all sets of data, isolation of spectral lines and observation of the continuum at 2.179 μm were achieved using a Fabry-Perot interferometer with a resolution of $\lambda/1000$, that is, ±150 kms^{-1}.

The northerly extent of the field which we were able to observe was restricted by the availability of only a single star, θ^1 B Ori, as a sufficiently bright reference for wavefront sensing. The field reported here consists of a single frame (12.″8×12.″8), centered 16.″8 E and 3.″4 S, relative to TCC0016 (see Fig. 1) and chosen for its strong $v = 2{-}1$ emission. The Strehl ratio, the ratio of the peak intensity of the measured point-spread function (PSF) to the theoretical maximum for a telescope with perfect optics and no atmosphere, diminishes as the distance from the reference star increases. θ^1 Ori B lies at the south-eastern corner of our image, with the north-west corner of our field ∼45″ away. This corresponds to a size of the order of that of the isoplanatic patch at 2 μm, the area beyond which AO correction may be significantly degraded. The size of the isoplanatic patch depends on the outer scale of turbulence, a poorly characterized parameter, and much larger isoplanatic patches have been reported. It turned out that the excellent seeing at the time of our observations allowed us to achieve mean-diffraction limited correction throughout the field, including faint objects. The resolution in our images corresponds to a Strehl ratio between 0.37 and 0.5. In order to obtain a representative point spread function, we chose to record θ^1 Ori D to the SE (see Fig. 1), rather than θ^1 Ori B, since θ^1 Ori D lies at a distance from our field more representative for the full field than θ^1 Ori B. Numerous observations were performed of θ^1 Ori D throughout data taking, since it is important for data reduction to use a PSF appropriate to the time of and therefore the seeing for any particular image acquisition.

Data reduction to obtain a H_2 image was performed so as to take account of any temporal variability of the sky background, spatial variations in the sensitivity of the detector (flat-fielding), differences in the sky brightness at different wavelengths and differing efficiencies of the detection system for the different Fabry-Perot settings. Dark counts were subtracted and bad pixels and noise due to cosmic rays removed.

Since we seek to ratio the images in $v = 1{-}0$ and $v = 2{-}1$ S(1), it is essential that brightness estimates are as free as possible from differential effects between the two lines. In this regard atmospheric absorption in these lines must be considered. Data obtained (Dec. 2000) on the Canada-France-Hawaii Telescope, using a combination of the PUEO adaptive optics system and Fabry-Perot interferometry ("GriF"; Clénet et al. 2002), as well as extensive data in Chrysostomou et al. (1997), reveal that OMC1 as a whole contains H_2 emission which shows velocity shifts, relative to Earth, of between +60 to −10 km s^{-1}. Using the atmospheric absorption line atlas of Livingston & Wallace (1991), we find that there is negligible absorption for the $v = 1{-}0$ line in all cases, save over a very narrow range of velocities around +30 kms^{-1} for which an absorption of ∼7% is found. For the $v = 2{-}1$ line, the situation is similar with a weak absorption feature again of ∼7% at around +33 kms^{-1}. GriF data show that the regions studied span the range of velocity which includes these values. Thus differential absorption

may introduce systematic errors into estimates of excitation temperature, but of only a few per cent. The effect cannot be accurately determined and we choose to ignore it in the present work.

A further consideration is that the $v = 2{-}1$ line will be less reddened than the $v = 1{-}0$ line. The factor between the two is $\sim(\lambda_1/\lambda_2)^{-1.7}$ (Mathis 1990), that is, the $v = 2{-}1$ line may be overestimated by ~10% compared to the $v = 1{-}0$ line. We present results here for data uncorrected for this imprecisely known differential absorption. If included, excitation temperatures estimated below would be reduced by ~5%. Absolute values of brightness may however be underestimated due to dust obscuration (Rosenthal et al. 2000), but this does not in itself affect estimation of excitation temperatures.

Data for the $v = 2{-}1$ S(1) line and at 2.179 μm in the continuum, free from H_2 emission, were deconvolved with the appropriate point-spread functions, using the technique of Subtractive Optimally Localized Averages, SOLA (Pijpers 1999). This method has been shown to preserve the smallest scales in the data more effectively than the standard methods of Maximum Entropy and Richardson-Lucy (Vannier 2001; Hook 1999 and references therein), yielding otherwise very similar results. Implementation of SOLA involves as input some "target" resolution which it is the aim of deconvolution to achieve. If this target represents too high a resolution, the penalty will be an unacceptable level of noise. In the present data we were able, with acceptable noise, to achieve a spatial resolution, uniform within the image, of 0.″15. Absolute fluxes were obtained by calibration using both the standard star HD71264, at $08^h26^m18^s.15$, –05°51′49.″8 (J2000), with a K magnitude of 8.538 (DENIS Standard Stars: see `http://cdsweb.u-strasbg.fr/denis.html`) and TCC0016, whose K' band calibration is given in McCaughrean & Stauffer (1994). Images of the $v = 2{-}1$ S(1) emission were obtained by subtraction of the deconvolved continuum image at 2.179 μm from that at 2.247 μm, noting that the continuum itself shows very little emission save that from stars in the field. The region is strongly illuminated by the Trapezium stars (see below) and absence of continuum emission indicates that very small dust particles, which show bright K-band emission in photon dominated regions (PDRs: e.g. NGC 7023: Lemaire et al. 1996), are absent in this part of OMC1 (Ferland 2001). Images extracted in the same manner as described above, but for the $v = 1{-}0$ S(1) line, may be found in V2001.

Excitation temperature images were created by forming a ratio of the $v = 2{-}1$ and $v = 1{-}0$ S(1) images. This places a stringent requirement on registration of the separate images. Two stars in the field were used for image registration, namely PSH132 and TCC0044 located 19″E, 3″N and 14″E, 7″S respectively of TCC0016 (see Fig. 1). Cuts through these stars show that superposition of the two sets of data may be performed with an accuracy of ±1 pixel on the full field. Thus ratio images could be made without significant loss of spatial resolution. (Data recently acquired using the Canada-France-Hawaii Telescope have enabled us to perform registration of $v = 2{-}1$ and 1–0 S(1) images using 10 stars in the field. Results confirm the registration of the images presented here.)

Referring to $v = 1$, $J = 3$ as level 1 and $v = 2$, $J = 3$ as level 2, both of the same degeneracy, the excitation temperature may be expressed as

$$T_{\rm ex} = \frac{E_2 - E_1}{k \ln \frac{n_1}{n_2}} \quad (1)$$

where $E_2 - E_1 = 3892.4$ cm^{-1}, and n_i are the populations of level $i = 1, 2$. The column densities, N_i, and hence the relative populations can be obtained from the observed brightness, I_i, using

$$N_i = \frac{4\pi\lambda_i}{hc}\frac{I_i}{A_i} \quad (2)$$

where λ is the wavelength and A is the Einstein A-value for the corresponding line (3.47×10^{-7} s^{-1} for $v = 1{-}0$ S(1) and 4.98×10^{-7} s^{-1} for $v = 2{-}1$ S(1); Wolniewicz et al. 1998).

The resulting H_2 excitation image can be seen in Fig. 2. To avoid unacceptable levels of noise in forming this image, all emission in the $v = 1{-}0$ and $v = 2{-}1$ S(1) lines weaker than 7×10^{-7} Wm^{-2} sr^{-1} (~10% of the maximum in the 2–1 line and ~2% of the maximum in the 1–0 line) was excluded. Details of two illustrative objects within Fig. 2 are shown in Figs. 3 and 4, which also show the corresponding $v = 1{-}0$ and $2{-}1$ data. The data show surprisingly clear excitation structure, ranging from excitation temperatures of 1500 K to >5000 K. There is a tendency for the emitting clumps of H_2 to show a hot edge. In addition, edges have a clear propensity to face south to southwest.

Cuts through objects 1 and 2 are shown in Figs. 5a, b, which illustrate that the excitation temperature in these zones can rise to more than 5000 K. Errors in the excitation temperatures quoted here and subsequently are ±10% for 3σ. Values of $T_{\rm ex}$ in hot zones lie in general around 3500 K to 4000 K. In cooler zones, values of $T_{\rm ex}$ congregate around 2500 K. A significant feature is that the edge of hot zones tends to be very abrupt, as shown in Fig. 5b.

A comparison may be made between excitation temperatures reported here and the excitation temperature(s) deduced from Boltzmann plots, that is, of (N_i/g_i) vs. E_i, where N_i is the column density of level i, and g_i and E_i the multiplicity and energy of level i respectively, using the ISO-SWS data of Rosenthal et al. (2000). The latter data integrate the emission in an area in the plane of the sky of ~15″ by 30″ in the region of Peak 1. This region, lying to the north of IRc2 (see Fig. 1) and about 3 times larger than the present region, suffers excitation processes similar in nature to those in Peak 2. The excitation temperature in the range of energies including $v = 2$, $J = 3$, spatially averaged over the ISO-SWS beam, is of the order of 3000 K in Rosenthal et al. (2000) or 3300 K according to Le Bourlot et al. (2002). It is evident therefore that the hot zones observed in the present work, very small on the scale of the ISO-SWS beam, are rather hotter than in general for OMC1 and represent a different set of physical conditions than the average for OMC1 as a whole.

Absolute values of brightness of H_2 emission in hot and cold zones in Figs. 2–4 provide an additional diagnostic of the prevalent physical conditions. The average value of brightness

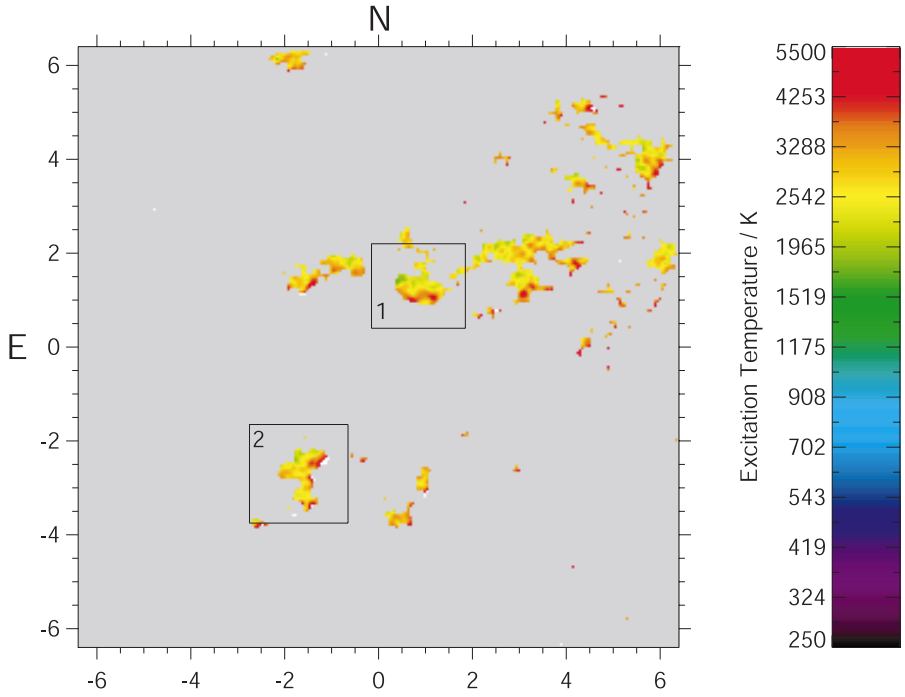

Fig. 2. An "excitation image" of the 12.″8 × 12.″8 region of OMC1, identified in Fig. 1, represented by an image of the excitation temperature as estimated using Eqs. (1) and (2). The centre of the image, designated (0,0), is located at $05^h35^m16\overset{s}{.}03$, –05°22′46.″7 (J2000), displaced 16.″8 E and 3.″4 S from the (0,0) position (TCC0016) in Fig. 1. The area in grey represents regions in which emission is below specified signal levels (see text). Boxes labelled 1 and 2 refer to data in Figs. 3 and 4.

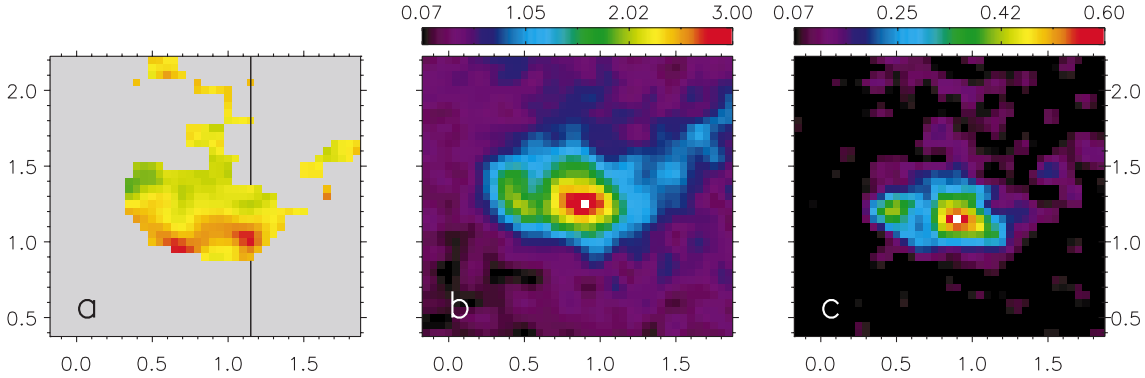

Fig. 3. a) A detail of region 1, identified in the excitation image in Fig. 2, **b)** corresponding emission in $v = 1{-}0$ S(1) and **c)** in $v = 2{-}1$ S(1). The line in Fig. 3a indicates the position of the cut taken in this image to form the data shown in Fig. 5a. The colour bars for brightness in **b)** and **c)** are in units of 10^{-5} Wm^{-2} sr^{-1}

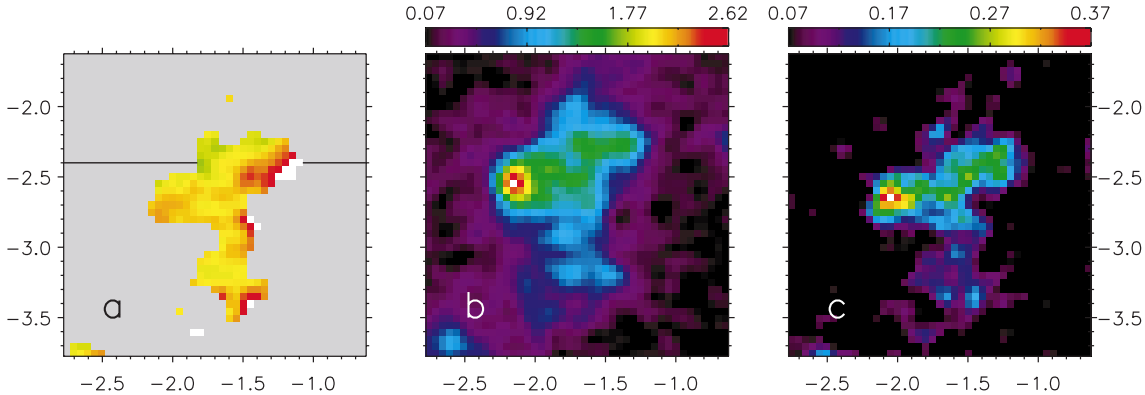

Fig. 4. As in Fig. 3, but for region 2, see Fig. 2. The line in **a)** indicates the position of the cut taken in this image to form the data shown in Fig. 5b. The colour bars for brightness in **b)** and **c)** are in units of 10^{-5} Wm^{-2} sr^{-1}

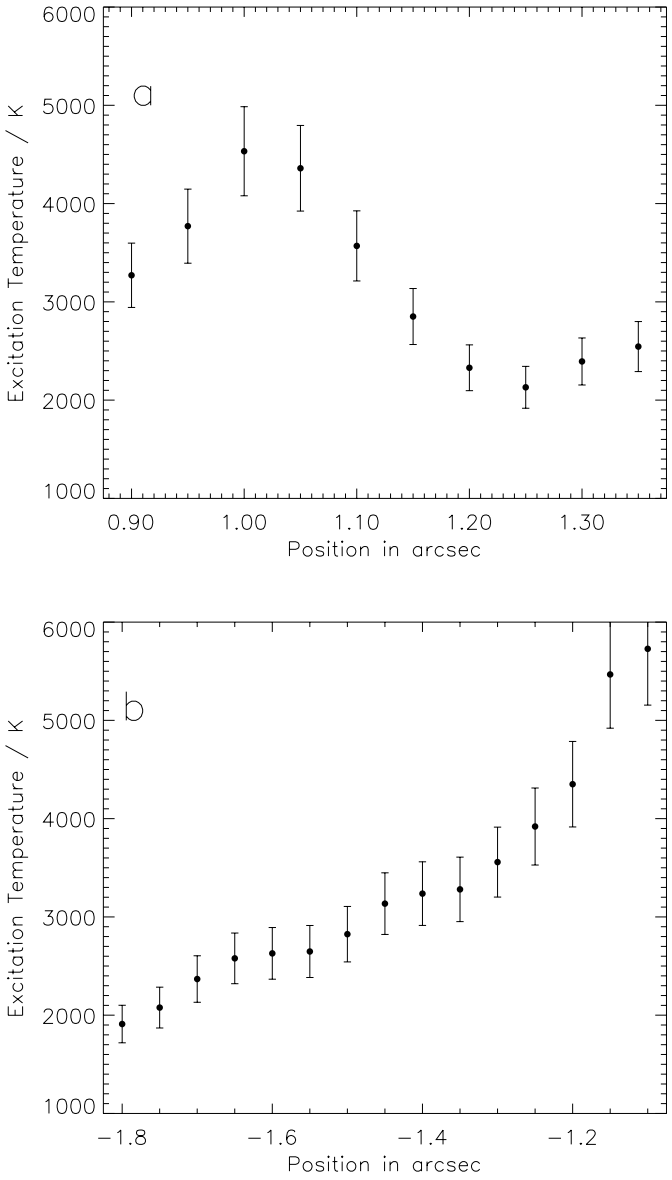

Fig. 5. a) A cut through the excitation image in Fig. 3a, region 1, in a direction N-S, 1.″15 west of the centre of the excitation image in Fig. 2, showing the variation of excitation temperature with position. **b)** A similar cut for region 2 in the E–W direction, 2.″4 south of the centre of the excitation image.

of the $v = 1{-}0$ S(1) line in hot zones with $T_{ex} > 3300$ K is $8.5 \pm 2.7 \times 10^{-6}$ Wm^{-2} sr^{-1} (1σ) whereas the cooler zones possess a higher brightness of between 1 and 3×10^{-5} Wm^{-2} sr^{-1}.

3. Discussion of the observations

H_2 emission in OMC1 arises from both heating through shocks (V2001 and see below), and from photon excitation in PDRs (Störzer & Hollenbach 1999 (SH99); Sternberg & Dalgarno 1989; Black & van Dishoeck 1987; Black & Dalgarno 1976). PDRs are characterized by high excitation temperatures, e.g. >5000 K for the S(1) $v = 2{-}1$ and 1–0 lines, at any rate for low number densities, that is, $\leq 10^4$ cm^{-3} (Sternberg & Dalgarno 1989). In the discussion that follows, we consider first the influence of shocks and then turn to the influence of the PDR generated by θ^1C Ori.

3.1. The influence of shocks

Our aim is to identify shock conditions which reproduce the observed range of excitation temperatures using shock models. Our discussion proceeds with the proviso that shock models do not yet yield a definitive description of the origin of H_2 emission. Indeed, models in general experience considerable difficulties in describing data for H_2 emission spectrum in such objects as the Orion bullets (e.g. Tedds et al. 1999).

Since the region may be permeated by magnetic fields (Norris 1984; Crutcher et al. 1999) and the gas is at least weakly ionized, shock models include not only J-type (Hollenbach & McKee 1989; Lim et al. 2002) and but also continuous-type (C-type) shock waves. The latter have been investigated by Draine et al. (1983), Pineau des Forêts et al. (1988), Smith & Brand (1990), Kaufman & Neufeld (1996a,b), Timmerman (1998), Wilgenbus et al. (2000), whose results were used in V2001, and most recently by Le Bourlot et al. (2002). The latter extends the work of Wilgenbus et al. (2000), showing that C-type shocks may propagate at considerably greater velocities than was previously believed, increasing the range from around 30 km s^{-1} to > 50 km s^{-1} depending on the gas density (see below). The model of Le Bourlot et al. (2002) used here abides by the relationship that the transverse magnetic induction is given by $B(\mu\text{G}) = [n(\text{cm}^{-3})]^{1/2}$, in contrast to the models reported for example in Smith (1991) and Smith et al. (1991) which invoke very high magnetic fields. Using the new model of Le Bourlot et al. (2002), the range of C-type shock speed and pre-shock gas density explored in the present work is therefore considerably enlarged over that investigated using the results of Wilgenbus et al. (2000) in V2001. The range of densities and shock speeds covers preshock values of $n = 10^3$ cm^{-3} to 10^7 cm^{-3} and shock speeds of 10 km s$^{-1} \leq v_{\text{shock}} \leq v_{\text{crit}}$, where v_{crit} is the maximum velocity at which a C-type shock is able to propagate in the medium for any chosen pre-shock density, ranging from $\geq$50 km s^{-1} for $n = 10^3$ cm^{-3} to ~24 km s^{-1} for $n = 10^7$ cm^{-3}. The steady-state code treats, in planar geometry, the hydrodynamics of the shock and the detailed chemistry in a self-consistent manner, including for example the chemistry-dependent cooling of the post-shock gas. Level population densities of H_2 ro-vibrational states are computed, in parallel with the chemical and dynamical variables. In the models to which we refer below, the ortho/para H_2 ratio is assumed to be 3 in the pre-shocked gas. We note that these latest shock models, which include the most recent collisional cross-section data (Le Bourlot et al. 2002), overcome the difficulties experienced in earlier shock models (e.g. Burton et al. 1990) in treating high density regions of $>10^5$ cm^{-3}.

We initially consider the possibility that in any clump, such as those in Figs. 3 and 4, we are observing generic structure in the emission of a shock, seen edgeways on, and that the observed excitation temperature structure reflects the cooling profile of the shock itself. In this physical model, observations

require that the width of the shocked region is of the order of a few hundred AU. This limits pre-shock densities to $<10^5$ cm^{-3}. In order to achieve a brightness in the S(1) $v = 1-0$ line in excess of 10^{-5} Wm^{-2} sr^{-1}, this turns out to require velocities of 40–50 km s^{-1}. Computed excitation temperature profiles however show $T_{\rm ex}$ remaining roughly constant, at 2600 K to 2800 K, throughout the emitting zone. Hence excitation temperature profiles do not resemble those observed (Figs. 5a, b) and we conclude that this edgeways-view model is not correct.

Turning first to a suitable model for the high $T_{\rm ex}$ zones, a large range of C- and J-type shocks has been explored in order to try to reproduce the high observed excitation temperatures. For C-type shocks, the only group which yield $T_{\rm ex}$ of 3500–4000 K are those which involve shock velocities of 25 to 30 km s^{-1} impinging on gas at a pre-shock density of 5×10^6 cm^{-3} (or higher, but with correspondingly lower shock velocities). For example, a shock velocity of 28 km s^{-1} in gas of pre-shock density 5×10^6 cm^{-3} yields $T_{\rm ex} = 3800$ K and a post-shock density of 1.1×10^8 cm^{-3} at 10 K. However the calculated brightness in the $v = 1-0$ S(1) line is 7×10^{-5} Wm^{-2} sr^{-1}, whereas the observed average brightness is ∼10 times lower. We find no C-type shocks which yield a high excitation temperature accompanied by the observed lower brightness, that is, lower brightness than in low $T_{\rm ex}$ zones.

Slower J-type shocks turn out to be better candidates to describe high excitation temperature zones. It is possible to identify a limited range of J-shock velocities and pre-shock densities which yields the observed excitation temperature and a suitable H_2 emission brightness. For example a J-type shock of velocity 15 km s^{-1}, impinging on pre-shock gas at a density of 10^6 cm^{-3}, yields a brightness in the $v = 1-0$ S(1) line of 3.4×10^{-6} Wm^{-2} sr^{-1} and in $v = 2-1$ S(1) of 1.0×10^{-6} Wm^{-2} sr^{-1}. This corresponds to $T_{\rm ex} = 3650$ K, representative of hot zones. The post-shock density at 50 K is estimated to be 1.5×10^8 cm^{-3}. This and similar shock models provide a brightness between 2 and 3 times less than the observed average value of 8.5×10^{-6} Wm^{-2} sr^{-1} in the 1–0 S(1) line. A higher preshock density may be chosen to yield the observed figure. However, as we describe in section 3.2, there is a PDR contribution to the emission of comparable magnitude to that provided by the shock and the uncertainties in both the shock and PDR models do not warrant more detailed estimates of shock speeds and densities. Despite this complexity, the $v = 2-1/1-0$ S(1) line ratio appears to be a good diagnostic of the physical conditions in the sense that high $T_{\rm ex}$ clearly implies high pre- and post-shock gas densities. The model width of the J-shocks mentioned above is a small fraction of 1 AU. Thus we postulate that the medium is under continuous shock excitation and is subject to a large number of small scale shocks, since these features together would yield the extended emission observed.

As described in V2001, which used the models described in Wilgenbus et al. (2000), C-type shocks are essential to reproduce the level of $v = 1-0$ S(1) emission in the brightest regions. Thus the brightly emitting zones of low excitation temperature, where the greatest $v = 1-0$ S(1) emission is found, can be modelled as C-type shocks involving pre-shock densities of the order of 10^6 cm^{-3}, post shock densities of a few $\times10^7$ cm^{-3} at 10 K, with accompanying shock velocities of 25–30 km s^{-1}. The observed 1–0/2–1 line ratio in cooler parts of region 1, for example, is 7.0 ± 0.3 around the peak of emission. The C-type shock models mentioned yield results which span this range, running from 9.6 to 5.0 or $T_{\rm ex} = 2200$ to 2900 K. Models predict a brightness in the $v = 1-0$ S(1) line of 3 to 6×10^{-5} Wm^{-2} sr^{-1} and are therefore also consistent with or a little brighter than values recorded in our observations.

In the shock interpretation outlined above, the excitation image is seen effectively to trace gas density and we conclude that clumps of material possess very dense regions. Using the scale size of $3.5 \pm 0.5 \times 10^{-3}$ pc derived in V2001, it was shown in V2001 on the basis of the Jeans length that gravitational instability may set in for number densities in excess of $\sim10^7$ cm^{-3}, for the largest of the clumps (region 1 in Fig. 2). It now appears that parts of this and other objects possess albeit small regions with number density of several times 10^8 cm^{-3} and therefore that the total mass contained within these clumps is somewhat larger than previous estimates of ∼0.1 $M_\odot$. This strengthens the conclusion of V2001 that region 1, for example, may contain sufficient material for low mass star formation.

In this connection, a new element in our interpretation arises from spatially and velocity resolved GriF data for H_2 emission in OMC1 (see Sect. 2; Gustafsson et al. 2003). We interpret these data as showing evidence that some of the OMC1 clumps may already possess protostars buried within them. Since outflow is characteristic of protostars (André et al. 1993; Evans 1999; Eislöffel et al. 2000), these clumps therefore suffer shocks originating from flows within the clumps rather than from an external source alone, such as the well characterised outflow from the BN-IRc2 zone (Doi et al. 2002). If a clump contains a protostar, H_2 emission then represents a later post-collapse stage of star formation, rather than the hastening of star formation through shock accumulation of dense material prior to gravitational collapse.

3.2. The influence of θ^1C Ori

The region observed is exposed to the far-UV radiation field of the Trapezium stars, of which the dominant contributor is the O-star θ^1C Ori, ∼0.09 pc distant from the H_2 emitting clumps. We initially set aside the high densities that arise in the shock model of Sect. 3.1 and consider purely PDR excitation.

θ^1C Ori generates a radiation field of $2–3 \times 10^5$ times the standard interstellar field ($G_0 = 2-3\times10^5$), including appropriate attenuation by dust in the HII outflow, as discussed in SH99. We note that estimates of G_0 could be too low by an order of magnitude (Ferland 2001), but that predictions of PDR models are insensitive to variation of G_0 over this range (SH99). With $G_0 = 2.5\times10^5$, $n = 4\times10^6$ cm^{-3}, including 2.6 km s^{-1} of advective heating, SH99 reports a brightness of 4.2×10^{-6} Wm^{-2} sr^{-1} in the $v = 1-0$ S(1) line. This is ∼7 times lower than the brightness of the central 0.″8 of region 1, for example (V2001). With the same model parameters, the $v = 2-1$ line brightness predicted in SH99 is 3.8×10^{-7} Wm^{-2} sr^{-1}, whereas the observed is $\sim5 \times 10^{-6}$ Wm^{-2} sr^{-1}. Results in SH99 correspond to an excitation temperature of ∼2000 K. Data in SH99 represent the most extreme PDR conditions which have been explored and

thus no known PDR model can account for the present observations. There must nevertheless be a PDR contribution to the H_2 emission, as subsequently discussed.

In addition, θ^1C Ori can also generate a shock in the zone of interest. The mass loss rate of θ^1C Ori is $\sim 4 \times 10^{-7}$ $M_\odot$ yr^{-1} with a velocity of 1000 km s^{-1} (Howarth & Prinja 1989; O'Dell 2001). This corresponds however to an energy flux of material in the region of H_2 emission which is 2 to 3 orders of magnitude too small to drive the shocks described in Sect. 3.1. Thus shocks from θ^1C Ori cannot account for the structure observed in the excitation temperature image. Rather the form of this image arises because the H_2 emission zones represent dense clouds within an HII region, subject both to shocks and PDR excitation, as we now describe.

We combine the effects of shocks, discussed in Sect. 3.1, with the environment generated by θ^1C Ori. The general nature of this environment in the zone of interest has been extensively studied. The HII region associated with the Trapezium cluster is very well-documented and its morphology is known in detail (Ferland 2001; O'Dell 2001; Wen & O'Dell 1995). Following Wen & O'Dell (1995), the main wall of the HII region lies 0.15 to 0.2 pc beyond the region observed. This is corroborated, for example, by recent data in Takami et al. (2002), who describe the morphology of the HII zone around the Trapezium stars, using [FeII], HeI and Paβ lines as diagnostic of the presence of the HII region. These data show that the present region is overrun by the HII zone and thus that the clumps observed are dense fragments, surviving in the HII region around the Trapezium stars (O'Dell 2001). This is supported by the fact that high $T_{\rm ex}$ regions are generally sharp-edged, where the expansion of the HII zone is effectively inhibited by the high density. Thus we interpret the form of the excitation temperature images in terms of a combination of shocks, which build high density, and an intense far-UV photon field from the south, largely from θ^1C Ori, which scours away less dense material through photoevaporation. This latter aspect is analogous to the photoevaporation model of circumstellar disks, so-called "proplyds" (Henney & O'Dell 1999). Only dense gas survives when unshielded from θ^1C Ori – providing the mass reservoir is large enough. This gives a qualitative explanation for the generally southern facing morphology of the hot dense zones, pointing towards the Trapezium cluster.

In this combined photoevaporation-shock description, the radiation field of θ^1C Ori falls upon very dense material, with $n \geq 10^8$ cm^{-3}, 2 orders of magnitude denser than in proplyd photoevaporation models of SH99. In order to estimate the brightness generated in the H_2 lines for such a dense region, a PDR model has been run using $G_0 = 2.5 \times 10^5$ and number densities between 10^8 cm^{-3} and 7.5×10^8 cm^{-3}. This model, based on a code described in Abgrall et al. (1992), involves purely the fluorescence mechanism of excitation of H_2. We find that the model generates a surface brightness of 1.5 to 2×10^{-6} Wm^{-2} sr^{-1} in the $v = 1$–0 S(1) line and 6 to 7×10^{-7} Wm^{-2} sr^{-1} in the $v = 2$–1 S(1) line. Thus photon excitation makes a significant contribution to the H_2 emission brightness, very comparable with the J-type shocks discussed in Sect. 3.1 and yielding the same excitation temperature. Moreover since this PDR model does not include advective flow, which should be present, the true emission brightness due to the FUV field of θ^1C Ori will be greater than the estimates mentioned. These considerations largely remove the discrepancy between observation and calculated brightness, found for the J-shock alone, as discussed in 3.1.

The photoevaporation model proposed in SH99 may also provide some basis for our inference, drawn from shock models, that shocks are both C-type and J-type within closely lying regions. C-type shocks require the presence of transverse magnetic induction, whereas J-type assume that this is absent or that the degree of ionization in the region is negligible. SH99 (and references therein) show that the effects of an intense FUV field falling upon dense material is to generate a neutral outflow. One may speculate that neutral outflowing material may drag ions and electrons away with it, creating a zone of low ionization, relatively devoid of magnetic induction, in which J-type shocks may propagate. A further possibility is that shocks in high $T_{\rm ex}$ zones do not achieve a steady state and we are observing the J-type region which accompanies the developing C-type shock.

A further point arises which may stimulate new observations. The combination of shocks and a PDR as above would yield a velocity spectrum of H_2 showing a narrow line for the PDR, superposed on broader shock emission. Thus high spectral resolution spectro-imaging of these regions, with a spatial resolution of $\sim 0\farcs2$, would yield data which provide a useful test of the model proposed. Existing data in Chrysostomou et al. (1997) or Salas et al. (1999) is of sufficient spectral resolution but has a spatial resolution of no better than $\sim 1\farcs6$.

4. Concluding remarks

The observational data presented here for $v = 2$–1 S(1) H_2 emission provide evidence for highly structured excitation temperatures and densities in clumps of gas in Orion. In a fraction of the volume of these clumps, densities deduced from shock models are an order of magnitude higher than previous estimates in V2001, where the latter were based solely upon $v = 1$–0 S(1) emission. We propose that the density structure of the clumps, a few times 10^7 cm^{-3} in the bulk, but in excess of 10^8 cm^{-3} at the high excitation temperature south-facing edges, is dictated by a combination of energetic shock compression and radiative evaporation. The emission of H_2 is formed in the body of the clumps by C-type shocks. However at the edges, facing θ^1C Ori, emission is generated through roughly equal contributions from J-type shocks and the PDR created by the intense FUV field of θ^1C Ori. The radiation field competes with the shock-induced process of accumulation of material, stripping away less dense matter at the fringes of the clumps and leaving behind only very dense regions facing in the direction of the Trapezium stars.

Acknowledgements. DF, LEK and MG would like to acknowledge the support of the Aarhus Centre for Atomic Physics (ACAP), funded by the Danish Basic Research Foundation. DF would also like to acknowledge support received from the Observatoire de Paris Meudon during the period of this work. JLL and GC would like to acknowledge the support of the PCMI National Program, funded by the CNRS in cooperation with the CEA and IN2P3. We also wish to thank the

Directors and Staff of ESO and of the CFHT for making possible observations reported in this paper. Thanks are also due to F.P. Pijpers (Aarhus) for his help in implementing the deconvolution techniques used here and to C.Nehme (Observatoire de Paris-Meudon) for running the PDR codes mentioned in the text.

References

Abgrall, H., Le Bourlot, J., Pineau des Forêts G., et al. 1992, A&A, 253, 525
Allen, D. A., & Burton, M.G. 1993 Nature, 363, 54
André, P., Ward-Thompson, D., & Barsony, M. 1993, ApJ, 406, 122
Bally, J., O'Dell, C. R., & McCaughrean, M.J. 2000, AJ, 119, 2919
Beckwith, S., Persson, S. E., Neugebauer, G., & Becklin, E. E. 1978, ApJ, 223, 464
Black, J. H., & Dalgarno, A. ApJ, 1976, 203, 132
Black, J. H., & van Dishoeck, E. F. 1987, ApJ, 322, 412
Boss, A. P. 2001, ApJ, 551, L167
Burton M. G., Hollenbach, D. J., & Tielens, A. G. G. M. 1990, ApJ, 365, 620
Chen, H., Bally, J., O'Dell, C. R., et al. 1998, ApJ, 492, L173
Chrysostomou, A., Burton, M. G., Axon, D. J., et al. 1997, MNRAS, 289, 605
Clénet, Y., Le Coarer, E., Joncas, G., et al. 2002, PASP, 114, 563
Crutcher, R. M., Troland T. H., Lazareff, B., Paubert, G., & Kazes, I. 1999, ApJ, 514, L121
Doi, T., O'Dell, C. R., & Hartigan, P. 2002, AJ, 124, 445
Draine, B. T., Roberge, W. G., & Dalgarno, A. 1983, ApJ, 264, 485
Eislöffel, J., Mundt, R., Ray T. P., & Rodriguez, L. F. 2000, Protostars and Planets IV, ed. V., Mannings, A. P., Boss, & S. S., Russeell (Tucson: University of Arizona Press)
Elmegreen, B. G., & Lada, C. J. 1977, ApJ, 214, 725
Evans, N.J. 1999, ARA&A, 37, 311
Ferland, G. J. 2001, PASP, 113, 41
Gezari, D. Y., Backman, D. E., & Werner, M. W. 1998, ApJ, 509, 283
Gustafsson, M., Kristensen, L. E., Clénet Y., et al. 2003, A&A, 411, 437
Henney, W. J., & O'Dell, C. R. 1999, Astron. J., 118, 2350
Hillenbrand, L. A. 1997, AJ, 113, 1733
Hollenbach, D. J., & McKee, C.F. 1989, ApJ, 342, 306
Hook, R. N. 1999, ST-ECF Newsletter, 26, 3
Howarth, I. D., & Prinja, R. K. 1989, ApJS, 69, 527
Kaufman, M. J., & Neufeld, D. A. 1996, ApJ, 456, 250
Kaufman, M. J., & Neufeld, D. A. 1996, ApJ, 456, 611
Le Bourlot, J., Pineau des Forêts, G., Flower, D. R., & Cabrit, S. 2002, MNRAS, 332, 985
Lemaire, J.-L., Field, D., Gerin, M., et al. 1996, A&A, 308, 895
Lim, A. J., Raga, A. C., Rawlings, J. M. C., & Williams, D. A., 2002, MNRAS, 335, 817
Livingston & Wallace 1991, An Atlas of the Solar Spectrum in the Infrared, N.S.O. Technical Report No.91-001, National Optical Astronomy Observatories, Tucson
Luhman, K. L., Rieke, G. H., Young, E. T., et al. 2000, ApJ, 540, 1016
Lucas, P. W., & Roche, P. F. 2000, MNRAS, 314, 858
Mathis, J. S. 1990, ARA&A, 28, 37
McCaughrean, M. J., & Stauffer, J. R. 1994, AJ, 108, 1382
Norris, R. P. 1984, MNRAS, 207, 127
O'Dell, C. R. 2001, ARA&A, 39, 99
Palla, F., & Stahler, S. W. 1999, ApJ, 525, 772
Pijpers, F. P. 1999, MNRAS, 307, 659
Pineau des Forêts, G., Flower, D. R., & Dalgarno, A. 1988, MNRAS, 235, 621
Rosenthal, D., Bertoldi, F., & Drapatz, S. 2000, A&A, 356, 705
Salas, L., Rosado, M., Cruz-Gonzales, I., et al. 1999, ApJ, 511, 822
Schild, H., Miller, S., & Tennyson, J. 1997, A&A, 318, 608
Schultz, A. S. B., Colgan, S. W. J., Erickson, E. F., et al. 1999, ApJ, 511, 282
Smith, M. D. 1991, MNRAS, 252, 378
Smith, M. D., & Brand, P. W. J. L. 1990, MNRAS, 242, 495
Smith, M. D., Brand, P. W. J. L., & Moorhouse A., 1991, MNRAS, 248, 730
Sternberg, A., & Dalgarno, A. 1989, ApJ, 338, 197
Stolovy, S. R., Burton, M. G., Erickson, E. F., et al. 1998, ApJ, 492, L151
Störzer, H., & Hollenbach, D. J. 1999, ApJ, 515, 669
Takami, M., Usuda, T., Sugai, H., et al. 2002, ApJ, 566, 910
Tedds, J. A., Brand, P. W. J. L., & Burton, M. G. 1999, MNRAS, 307, 337
Timmerman, R., 1998, ApJ, 498, 246
Vannier, L., Lemaire, J. L., Pineau des Forêts, G., et al. 2000, Atomic and Molecular Data for Astrophysics: New Developments, Case Studies and Future Needs, 24th meeting of the IAU, Joint Discussion 1, August 2000, Manchester, England, vol. 1, p. 56
Vannier, L., Lemaire, J. L., Field, D., et al. 2001, A&A, 366, 651
Vannier, L. 2001, Ph.D. Thesis, Observatoire de Paris-Meudon and Université Cergy-Pontoise
Wen, Z., & O'Dell, C. R. 1995, ApJ, 438, 784
Wilgenbus, D., Cabrit, S., Pineau des Forêts, G., & Flower, D. R. 2000, A&A, 356, 1010
Wolniewicz, L., Simbotin, I., & Dalgarno, A. 1998, ApJS, 115, 293
Zapatero Osorio, M. R., Bejar, V. J. S., Martin, E. L., et al. 2000, Science, 290, 103